Synthetic Lethal Targeting of Superoxide Dismutase 1 Selectively Kills *RAD54B*-Deficient Colorectal Cancer Cells

Babu V. Sajesh,* Melanie Bailey,† Zelda Lichtensztejn,* Philip Hieter,† and Kirk J. McManus*,[1]

*Manitoba Institute of Cell Biology and Department of Biochemistry and Medical Genetics, University of Manitoba, Winnipeg, Manitoba, R3E 0V9, Canada and †Michael Smith Laboratories, Department of Medical Genetics, University of British Columbia, Vancouver, British Columbia, V6T 1Z4, Canada

ABSTRACT Synthetic lethality is a rational approach to identify candidate drug targets for selective killing of cancer cells harboring somatic mutations that cause chromosome instability (CIN). To identify a set of the most highly connected synthetic lethal partner genes in yeast for subsequent testing in mammalian cells, we used the entire set of 692 yeast CIN genes to query the genome-wide synthetic lethal datasets. Hierarchical clustering revealed a highly connected set of synthetic lethal partners of yeast genes whose human orthologs are somatically mutated in colorectal cancer. Testing of a small matrix of synthetic lethal gene pairs in mammalian cells suggested that members of a pathway that remove reactive oxygen species that cause DNA damage would be excellent candidates for further testing. We show that the synthetic lethal interaction between budding yeast *rad54* and *sod1* is conserved within a human colorectal cancer context. Specifically, we demonstrate *RAD54B*-deficient cells are selectively killed relative to controls via siRNA-based silencing and chemical inhibition and further demonstrate that this interaction is conserved in an unrelated cell type. We further show that the DNA double strand breaks, resulting from increased reactive oxygen species following SOD1 inhibition, persist within the *RAD54B*-deficient cells and result in apoptosis. Collectively, these data identify SOD1 as a novel candidate cancer drug target and suggest that SOD1 inhibition may have broad-spectrum applicability in a variety of tumor types exhibiting *RAD54B* deficiencies.

UNDERSTANDING the pathogenic origins of colorectal cancer (CRC) is critical to develop the next generation of therapeutic strategies and targets. Chromosome instability (CIN) is characterized by increased frequencies of numerical and structural chromosomal aberrations (Lengauer *et al.* 1998) and is prevalent within a large fraction of tumor types. CIN not only drives tumorigenesis (Lengauer *et al.* 1998) but is associated with poor prognosis (Gao *et al.* 2007; Heilig *et al.* 2010) and the acquisition of multidrug resistance (Lee *et al.* 2011). CIN has been studied in CRC where it is an early event in the pathogenesis of the disease (Shih *et al.* 2001) and is found in up to 85% of sporadic tumors (Rajagopalan *et al.* 2004). Although the somatic gene mutations that drive CIN remain largely unknown, it is clear that no single gene is responsible for the CIN phenotype observed in CRCs. Rather, the entire mutational spectrum that underlies CIN is accounted for by a set of genes, with each individual gene typically representing <4% of the entire spectrum (Rajagopalan *et al.* 2004; Wang *et al.* 2004; Barber *et al.* 2008; Cancer Genome Atlas Network 2012). Gene resequencing efforts have identified several candidates involved in chromosome segregation, DNA replication, and DNA repair that are somatically mutated or deleted in a subset of sporadic CRCs exhibiting CIN (Wang *et al.* 2004; Sjoblom *et al.* 2006; Barber *et al.* 2008; Cancer Genome Atlas Network 2012). CIN therefore represents a defining characteristic that distinguishes cancerous from normal cells and it is within this feature, where we believe that potential exists to identify novel therapeutic targets capable of selectively killing cancer cells.

Hartwell *et al.* (1997) posited that cancer cells harboring specific somatic mutations may be selectively killed by targeting or inhibiting a second unlinked gene target through

doi: 10.1534/genetics.113.156836
Manuscript received July 19, 2013; accepted for publication August 25, 2013
Available freely online through the author-supported open access option.
Supporting information is available online at http://www.genetics.org/lookup/suppl/doi:10.1534/genetics.113.156836/-/DC1.
[1]Corresponding author: Manitoba Institute of Cell Biology, ON6010-675 McDermot Ave., Winnipeg, MB, R3E 0V9, Canada. E-mail: mcmanusk@cc.umanitoba.ca

a synthetic lethal (SL) paradigm. Synthetic lethality refers to the lethal combination of two independently viable mutations and is well studied in model organisms such as the budding yeast. Indeed, several extensive screens have been performed in yeast (Tong *et al.* 2001; Pan *et al.* 2006) with the collective goal of generating a comprehensive list of SL interactors for all known yeast genes (*i.e.*, nonessential and essential). Through cross-species approaches, these yeast datasets can be exploited to identify candidate SL interactors of yeast CIN genes whose human orthologs are somatically mutated in CRC. Once validated in mammalian cells, these SL interactors will represent novel candidate drug targets. Recently, we showed that a SL interaction first observed in yeast (*rad54 rad27*) was conserved in a human CRC context (*RAD54B FEN1*, respectively) (McManus *et al.* 2009). We showed that *RAD54B*-deficient CRC cells, and not isogenic controls, were selectively killed following FEN1 silencing and thus validated FEN1 as a novel candidate drug target. Since this initial work, many additional studies in various model systems have been performed, suggesting that >50% of SL interactions among selected subsets of CIN genes observed in budding yeast are conserved in other model organisms (Tarailo *et al.* 2007; Dixon *et al.* 2008; McLellan *et al.* 2009).

To identify novel candidate therapeutic targets, we significantly expanded our initial cross-species candidate approach to uncover conserved SL interactors of CIN genes. Using the 692 yeast CIN genes (Yuen *et al.* 2007; Stirling *et al.* 2011) and publicly available yeast datasets, we assembled all known SL interactors to date of the yeast CIN gene set. Hierarchical clustering identified several data-rich regions including one that harbored an abundance of SL interactors of yeast CIN genes whose human orthologs are somatically mutated in CRC. Preliminary direct tests performed in human cells suggested that members of a pathway required to remove reactive oxygen species (ROS) would be excellent candidates for further study and specifically focused our attention on superoxide dismutase 1 (SOD1). Here we show that *RAD54B*-deficient cells and not isogenic controls are selectively killed following either SOD1 silencing or chemical inhibition. By expanding this work into an unrelated cell type, we show that the *RAD54B SOD1* SL interaction is evolutionarily conserved and independent of cell type. To address the mechanism of killing, we show that the DNA damage resulting from the increase in ROS following SOD1 inhibition persists within the *RAD54B*-deficient cells and is associated with apoptosis. Thus, our data strongly suggest that SOD1 is a novel candidate therapeutic target for CRCs and perhaps other tumor types harboring *RAD54B* defects.

Materials and Methods

Network generation and testing

For gene clustering, all known negative genetic, synthetic lethal, and synthetic growth defects (collectively referred to in the text as SL) involving the 692 yeast CIN genes were identified in BioGRID (version 3.1.71). Interacting genes were sorted based on their total number of SL interactions regardless of interaction strength. It was not possible to perform statistical analyses to prioritize and select candidates as the strengths of the negative genetic interactions are typically qualitative measurements and experimental conditions are expected to differ significantly between the assays and the laboratories in which the experiments were performed. The top ~500 yeast genes were clustered with the 692 CIN genes using Cluster and viewed using Java TreeView. To directly test SL interactions in HCT116 cells, we used RNAi and previously established protocols (van Pel *et al.* 2013). For siRNA-mediated knockdown, cells were seeded in 6-well dishes 24 hr prior to transfection with 50 nM of single or double siRNA depending on the interaction tested. The next day, cells were detached, counted, and reseeded at low density in 96-well (six replicates) plates. After 5 days, cells were paraformaldehyde fixed and nuclei were counterstained with Hoechst 33342 and enumerated.

Cell culture

HCT116 (CRC) cells were purchased from American Type Culture Collection and grown in McCoy's 5A medium (HyClone) supplemented with 10% FBS. *RAD54B*-deficient HCT116 cells were generously provided by K. Miyagawa (Hiroshima University, Japan). Immortalized (telomerase) BJ normal human skin fibroblasts, hTERT, were generously provided by C. P. Case (Cogan *et al.* 2010) (University of Bristol) and were grown in DMEM (HyClone) containing 10% FBS. Cell lines were authenticated on the basis of recovery, viability, growth, morphology, and spectral karyotyping. RAD54B expression status was confirmed by Western blots prior to their use in experiments. All cells were grown in a 37° humidified incubator containing 5% CO_2.

Gene silencing

Cells were transiently transfected with siRNA duplexes using RNAiMax (Invitrogen) as detailed elsewhere (McManus *et al.* 2009). ON-TARGETplus siRNA duplexes targeting *SOD1*, *RAD54B*, *GAPDH*, and *PLK1* were purchased from Dharmacon and employed as either individual siRNAs (100 nM total) or pools that consisted of four different siRNAs (25 nM each or 100 nM total) targeting the same gene. The efficiency of gene silencing was confirmed by Western blot analyses.

Western blot analyses

Western blots were performed as detailed elsewhere (McManus *et al.* 2009) and blotted with RAD54B (Abcam ab83311; 1:1000), SOD1 (Abcam ab13498; 1:3000), and α-tubulin (Abcam ab7291; 1:10,000) antibodies. Protein knockdown efficiencies were evaluated through semiquantitative analyses of scanned blots using ImageJ (Gel Analyzer tool). All semiquantitative data were normalized to corresponding α-tubulin loading control for each lane.

Direct SL test

High content microscopy was used to evaluate the SL interactions a minimum of three times as detailed elsewhere

(McManus *et al.* 2009). Briefly, 8000 *RAD54B*-proficient or *RAD54B*-deficient HCT116, or 4000 hTERT cells were seeded into 96-well optical plates. Cells were transfected in sextuplet (*i.e.*, 6 wells per plate) with either individual or pooled siRNAs targeting *RAD54B*, *SOD1*, and controls (*GAPDH* and *PLK1*). *GAPDH* serves as a negative control (McManus *et al.* 2009), while *PLK1* is a positive control for cell death independent of any SL interaction (Spankuch-Schmitt *et al.* 2002), and also serves as an indicator of transfection efficiency. Cells were supplemented with 150 μl of normal growth medium 24-hr post-transfection, and permitted to grow for an additional 3 days (HCT116) or 4 days (hTERT), prior to paraformaldehyde fixation. Nuclei were counterstained with Hoechst 33342 (Sigma; 0.25 μM) and imaged. Nine central nonoverlapping images were acquired per well using a ×20 plan apochromat dry lens (numerical aperture = 0.8) on a Zeiss AxioObserver Z1 equipped with an LED Colibri light source and AxioVision v4.8 software. Images were analyzed using the Assaybuilder (physiology analyzer) within the AxioVision software. The total number of cells (Hoechst-positive nuclei) in each well was determined. All data were imported into Prism v5.0 (GraphPad), normalized to *GAPDH*-silenced controls, and statistical analyses were performed.

Dose response curves

Dose response curves were generated using a dilution series for ammonium tetrathiomolybdate (ATTM) and 2-methoxyestradiol (2ME2). Asynchronous cells (8000) were seeded into 96-well optical plates, and following attachment, the growth medium was supplemented with DMSO (vehicle control), ATTM, or 2ME2. Cells were permitted to grow for 3 days, fixed, counterstained with Hoechst, imaged, and analyzed as above. All data were imported into Prism v5.0 (GraphPad), normalized to DMSO-treated controls, and half maximal effective concentration (EC_{50}) values were determined. The EC_{50} values calculated for ATTM (4.2 μM) and 2ME2 (7.3 μM) in *RAD54B*-deficient cells were employed in all subsequent experiments.

Chemical SL test

Chemical SL tests were performed in an analogous fashion to the direct SL tests detailed above. However, ATTM and 2ME2 were employed in place of the si*SOD1* duplexes, while DMSO served as the vehicle control. Following a 3-day incubation period, cells were fixed and analyzed as above.

Real-time cell analyses

Real-**t**ime **c**ell **a**nalyses (RTCA) (*i.e.*, growth curves) were performed in quadruplicate using an RTCA-dual plate (DP) (Acea Biosciences). The RTCA-DP system employs microelectrodes at the bottom of each well to measure increases or decreases in electrical impedance (termed cell index) that reflect increases or decreases in cell numbers, respectively (Solly *et al.* 2004). Briefly, 8000 cells were seeded into each well of an E-Plate and growth was monitored in real-time every 10 min at 37°. DMSO, ATTM, and 2ME2 were supplemented into the medium when cell indices attained ~20–25% of their untreated maximum values (~24 hr postseeding) and growth was monitored for 3 additional days. All data were imported into Prism and **p**roliferation **d**efects were calculated as (PD = 1 − [Cell $Index_{Drug}$/Cell $Index_{DMSO}$]) × 100) for each cell line and treatment.

Colony-forming assay

A total of 10,000 cells per well were seeded in soft agar into a six-well plate in triplicate. Colonies were grown at 37° with media containing DMSO, ATTM, or 2ME2 replaced every 2 days. Following 28 days, cells were stained with 0.1% crystal violet and imaged using a 14-megapixel, charge-coupled device (CCD) digital camera. Total number of colonies per well was quantified using ImageJ (Analyze Particles and Measurement).

Detection of ROS

ROS were detected by employing Image-iT LIVE green ROS detection kit (Molecular Probes) by following the manufacturer's protocol with slight modifications to suit HCT116 cells. Briefly, RAD54B-proficient and RAD54B-deficient HCT116 cells were seeded onto sterile coverslips in each well of a six-well plate and allowed to grow at 37° for 24 hr. Semiconfluent cells on coverslips were treated with DMSO, ATTM, or 2ME2 for 6 hr. Following treatment, the cells were washed in warm Hank's balanced salt solution (HBSS) (37°) and were subsequently bathed in carboxy- 2′,7′-dichlorodihydrofluorescein diacetate (carboxy-H_2DCFDA) containing growth medium for 10 min at 37° in the dark. Subsequently, cells were washed three times in warm HBSS as before and coverslips were mounted onto glass slides in warm HBSS and cells were immediately imaged. Cells were counterstained with Hoechst 333342, by supplementing 1 μM Hoechst 333342 into the growth medium for 5 min before the initial wash with HBSS, after carboxy-H_2DCFDA treatment. Cells were imaged on a AxioImager 2 (Zeiss) equipped with an AxioCam high-resolution CCD camera (Zeiss) and a ×63 oil immersion plan apochromat lens (1.4 numerical aperture), using identical exposure times for each condition as previously described (McManus and Hendzel 2005). The experiment was repeated an additional two times.

Quantitative imaging microscopy

The presence of DNA double strand breaks was evaluated using an established quantitative indirect immunofluorescence-based approach (McManus and Hendzel 2005). Briefly, 8000 asynchronous cells were seeded into a 96-well plate and permitted to attach. Cells were treated with DMSO, ATTM, or 2ME2 for 6 hr, rinsed twice with PBS, and allowed to recover for 36 hr in drug-free media. Cells were fixed, permeabilized, labeled with either γ-H2AX (Abcam ab18311 at 1:2000) or 53BP1 (Abcam ab21083 at 1:200) antibodies and imaged using identical exposure times for each condition as described (McManus and Hendzel 2005). The mean

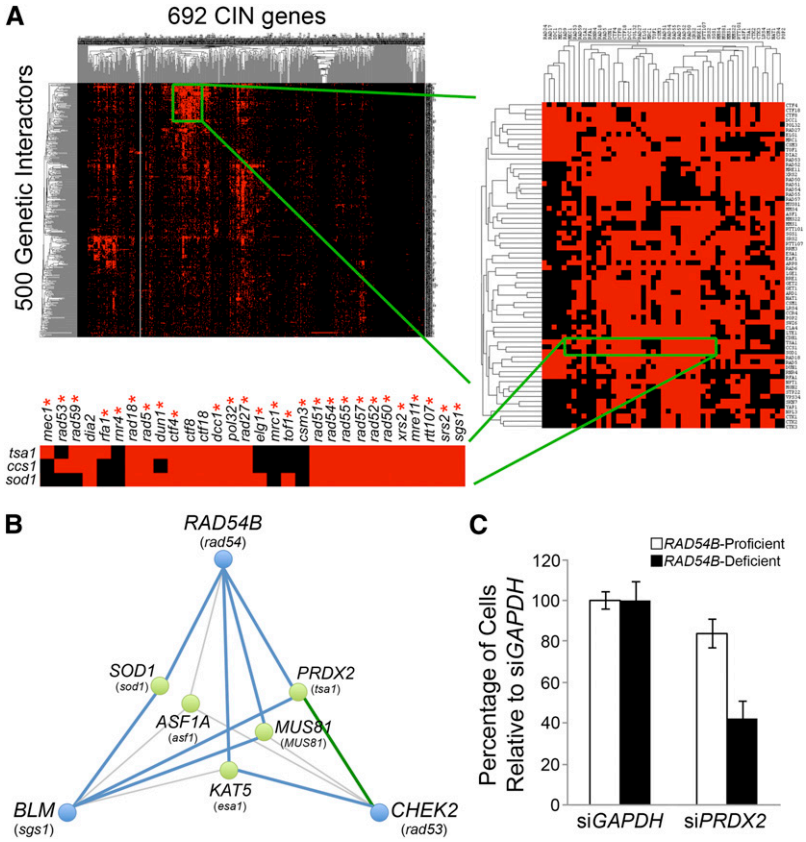

Figure 1 Analysis of yeast CIN gene SL interactions identify highly connected gene pairs. (A) Two-dimensional hierarchical gene clustering performed on 692 yeast CIN genes and their top 500 genetic interactors (left). A "data-rich" area of the clusterogram was used to identify a smaller (right) and highly focused network (bottom) of candidate interactions. Yeast *sod1* is a SL interactor with genes whose human orthologs are mutated or deleted in CRC (red asterisks and Table S1). Yeast *sod1* clusters with its copper chaperone, *ccs1* (human *CCS*), and another ROS detoxifying enzyme *tsa1* (human *PRDX2*). (B) Mini SL network comprising the human orthologs of yeast CIN genes (blue circles) that are somatically mutated in CRC and SL interactors evaluated in human cells (green circles). Putative conserved SL interactions are identified with a blue line, while those specific to yeast are shown in gray, and the single interaction identified only in HCT116 cells is shown in green. Human gene names are indicated with the corresponding yeast gene listed within parentheses. (C) Graphical depiction of a putative SL interaction observed between human *RAD54B* and *PRDX2*. Shown are the relative percentages of cells remaining ±SD, following siRNA treatments (*x*-axis). Note the enhanced killing (*i.e.*, lower percentage of cells remaining) in the *RAD54B*-deficient cells treated with siPRDX2 relative to controls.

γ-H2AX and 53BP1 total signal intensities were determined for each nucleus and normalized to the DAPI total signal intensity of the corresponding nucleus to account for differences in DNA content (McManus and Hendzel 2003). The induction of apoptosis was evaluated by examining the abundance of cleaved Caspase 3 (Abcam ab13847 at 1:2000). Cells were seeded as above and treated with DMSO, ATTM, or 2ME2 for 12 hr. Staurosporine (1 μM) was used as a positive control as it is an inducer of apoptosis. Cells were fixed, labeled, imaged, and analyzed as above. To account for differences in cell numbers, the cleaved Caspase 3 total signal intensity was determined for each nucleus and normalized to the corresponding DAPI signal intensity.

Results

Global SL data from yeast can predict highly connected interactions in humans with therapeutic potential

To identify potential SL interactors that are highly connected to CIN genes that are somatically mutated in CRC (*e.g.*, *RAD54B*), we used the yeast interaction data available in BioGRID. We queried the database for all known SL interactions for the entire set of 692 yeast CIN genes (Yuen *et al.* 2007; Stirling *et al.* 2011). A total of 4146 interactors were identified, which were subsequently prioritized based on the total number of interactions with the query CIN genes. Two-dimensional hierarchical clustering was performed between the CIN genes and the top ∼500 SL target genes (*i.e.*, those with ≥22 interactions; a threshold chosen arbitrarily) (Figure 1A, left). Several data-rich regions were identified, including one that harbored an abundance of SL interactions with DNA repair genes (Figure 1A, right), which were subsequently filtered, based on their connectivity within gene networks (Figure 1A, bottom). This most highly connected set of data held several DNA repair CIN genes (Supporting Information, Table S1), including *sgs1* (human *BLM*) and *rad54* (human *RAD54B*). The SL interactors of these CIN genes include many well-known DNA replication and repair factors such as the yeast Mre11/Rad50/Xrs2 complex (human Mre11A/Rad51/NBS1). In addition, the data-rich region also included all three members of a highly conserved pathway required to remove superoxide radicals (*i.e.*, ROS), yeast *tsa1*, *ccs1*, and *sod1*, whose human orthologs are *PRDX2*, *CCS*, and *SOD1*, respectively (Figure 1A, bottom).

A focused mininetwork was selected for preliminary testing in HCT116 (CRC) cells (Figure 1B), and using RNAi-based approaches and gene knockout cell lines with relevant controls, we determined that 53% (8/15) of the SL interactions tested appear to be conserved, including the *RAD54B SOD1* (yeast *rad54 sod1*) and *RAD54B PRDX2* (yeast *rad54 tsa1*) SL interactions (Figure 1C). SOD1 was specifically selected for subsequent testing as it encodes an enzyme that is highly conserved between yeast and humans (>70% similarity); its role in the removal of superoxide radicals is well established in both organisms; and SOD1 inhibitors have already been developed, some of which are currently being evaluated for

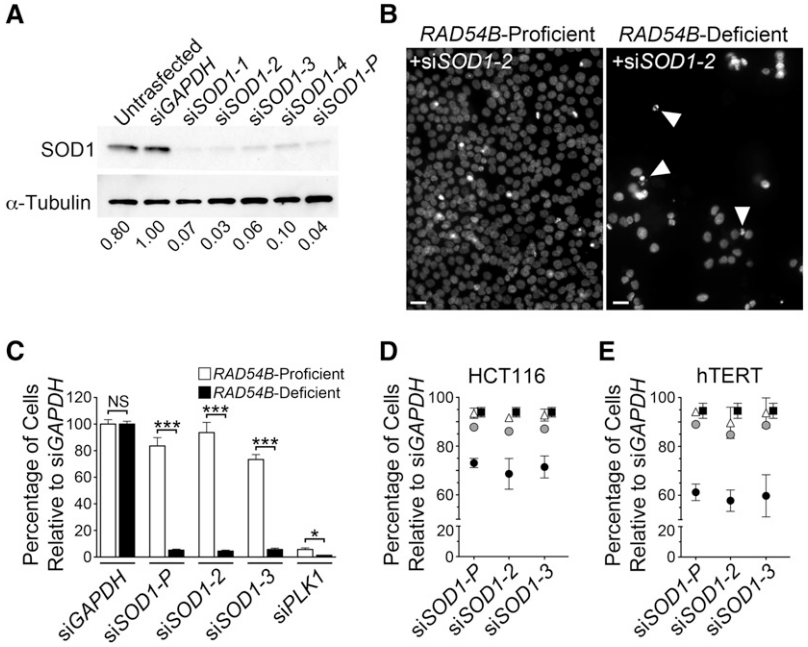

Figure 2 *RAD54B* and *SOD1* are synthetic lethal interactors in human cells. (A) Western blot depicting diminished SOD1 expression following siRNA-mediated knockdown in HCT116 cells; α-tubulin is a loading control. Semiquantitative analysis was performed and the normalized SOD1 expression levels relative to si*GAPDH* (1.00) are shown. (B) Representative images depicting the qualitative decrease in cell numbers (*i.e.*, DAPI-stained nuclei) following SOD1 silencing of *RAD54B*-deficient cells relative to controls. Arrowheads identify nuclei exhibiting hallmarks of cellular cytotoxicity. Bars, 25 μm. (C) Graphical depiction for the relative percentage of control and *RAD54B*-deficient cells (±SD) following treatment with various siRNAs (*x*-axis); statistical significance is indicated (***P-value <0.0001; *P-value <0.05; NS, not significant). Graphical depiction of the SL interaction observed following the simultaneous silencing of RAD54B and SOD1 in (D) *RAD54B*-proficient HCT116 and (E) hTERT cells. Depicted are the mean normalized percentages (±SD) for the individual silencing of either RAD54B (solid squares) or SOD1 (open triangles), and the expected value (shaded circles) calculated for the dual combined siRNAs calculated using a multiplicative model. Solid circles identify the actual observed values for the simultaneous dual silencing.

their ability to prevent angiogenesis in cancer (Juarez *et al.* 2006; Donate *et al.* 2008; Lowndes *et al.* 2009). Furthermore, since SOD1 is dispensable in both yeast (Chang *et al.* 1991) and mice (Kondo *et al.* 1997), it is likely that targeting SOD1 in a CRC context will have minimal effects on normal cells.

The budding yeast Rad54 Sod1 SL interaction is evolutionarily conserved in humans

We specifically chose to evaluate a potential SL interaction between *SOD1* and *RAD54B* because *RAD54B* is a chromosome stability gene (McManus *et al.* 2009) involved in homologous recombination repair (Miyagawa *et al.* 2002), which is somatically mutated in CRC (Cancer Genome Atlas Network 2012) and many additional tumor types (Forbes *et al.* 2011) (Table S1). We first evaluated the silencing efficiencies of SOD1 siRNAs (Figure 2A) and selected the two most efficient silencers (si*SOD1-2* and *-3*). Next, we employed our established siRNA-based approach using isogenic *RAD54B*-proficient (control) and *RAD54B*-deficient HCT116 cells (McManus *et al.* 2009) to validate the *RAD54B SOD1* SL interaction. As predicted, there was a visually striking decrease in the total number of *RAD54B*-deficient cells relative to controls (Table S2), following SOD1 silencing (Figure 2B), that were deemed statistically significant relative to controls (Figure 2C). Further inspection of the images revealed that a few remaining *RAD54B*-deficient cells exhibited hallmarks of cytotoxicity (*i.e.*, apoptosis) including chromatin condensation, nuclear blebbing, and fragmentation (Figure 2B, arrowheads) that were not apparent within the controls, while immunofluorescent labeling with a mitosis-specific marker (antiphosphorylated serine 10 of histone H3) confirmed the cells were not arrested in G2/M phase (data not shown).

Although the above data support an evolutionarily conserved SL interaction, it remained possible that the putative *RAD54B SOD1* interaction occurs due to a *de novo* background mutation that arose during the generation of the *RAD54B*-deficient cells. Consequently, we confirmed our ability to silence RAD54B and SOD1 (Figure S1A and Figure 2A) and performed dual siRNA experiments in *RAD54B*-proficient parental cells. As anticipated, the simultaneous silencing of *RAD54B* and *SOD1* resulted in a larger decrease in the relative percentage of cells than when either RAD54B or SOD1 are silenced alone (Figure 2D), or what is expected as calculated by a multiplicative model (Table S3). To extend our findings beyond a CRC context, similar dual siRNA tests were performed in a karyotypically stable, immortalized (telomerase) fibroblast cell line, hTERT (Figures S1B and C, Figure S2, and Table S4). As above, the simultaneous silencing of *RAD54B* and *SOD1* resulted in fewer cells than silencing either alone (Figure 2E), and a decrease in relative percentage of cells beyond that expected using a multiplicative model (Table S5). Collectively, these data suggest that the *RAD54B SOD1* SL interaction is evolutionarily conserved and is independent of cell type.

RAD54B-deficient cells hypersensitive to ATTM and 2ME2

Next, two chemical compounds were evaluated for their ability to phenocopy the RAD54B-specific killing identified above; ATTM is a SOD1 inhibitor that chelates Cu^{2+}, an essential cofactor required for its activity (Juarez *et al.* 2006), and 2ME2, which does not inhibit SOD1 *per se*, but rather induces the formation of ROS including superoxide radicals and thus mimics SOD1 inhibition (Huang *et al.* 2000; Kachadourian *et al.* 2001). Standard dose response curves (Figure 3A) revealed that *RAD54B*-deficient cells were >10-fold more sensitive to ATTM (EC_{50} = 4.2 μM) and 2ME2 (7.3 μM) treatments relative to controls (67.7 μM

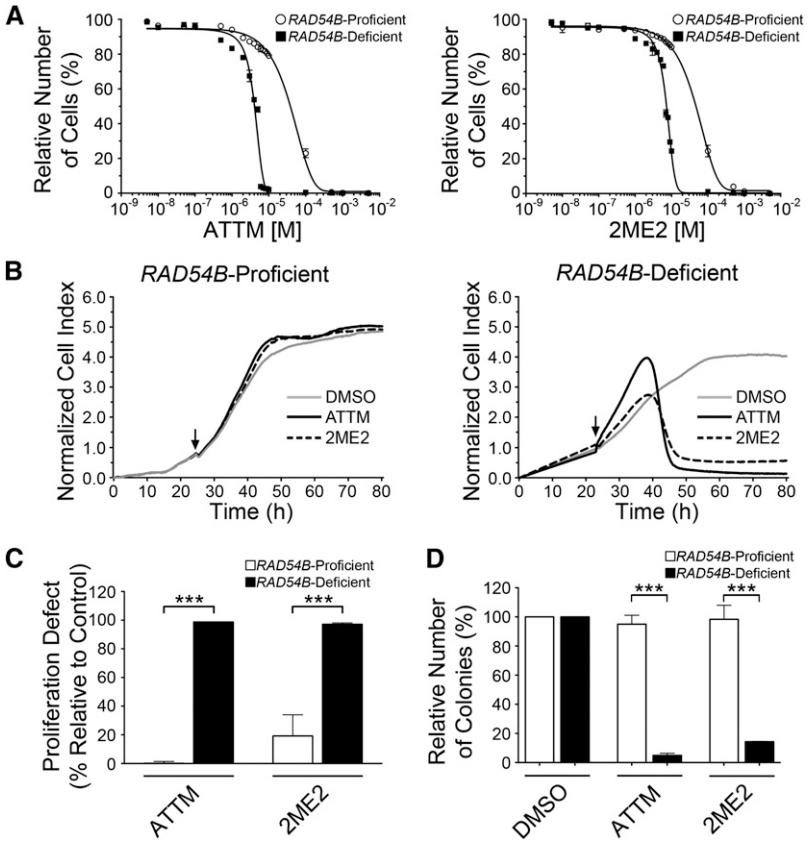

Figure 3 *RAD54B*-deficient cells are selectively killed following ATTM and 2ME2 treatment. (A) Dose response curves for cells treated with varying concentrations of ATTM (left) and 2ME2 (right). Data are normalized to the respective DMSO-treated controls. (B) Real-time growth curves for control (left) and *RAD54B*-deficient (right) cells treated with DMSO, ATTM, or 2ME2. Chemical compounds were added 20 hr postseeding (arrow). (C) Graph depicting an increase in the mean proliferation defects (±SD) for *RAD54B*-deficient cells treated with either ATTM or 2ME2 (*x*-axis), relative to controls. Student's *t*-tests identified highly statistically significant increases in mean proliferation defects (***P-value <0.0001) for the *RAD54B*-deficient treated cells. (D) Graphs depicting the relative number (±SD) of colonies formed in soft agar for cells treated with DMSO, ATTM, or 2ME2 for 28 days (***P-value <0.0001).

and 75.1 μM, respectively). Western blots confirmed that the drug sensitivities were not due to changes in SOD1 abundance following treatments (Figure S3).

Having established that ATTM and 2ME2 can functionally substitute for SOD1 siRNAs and recapitulate the *RAD54B* SL interaction, we now wished to determine if the treatments induced cell cycle arrest or cytotoxicity. Cellular growth rates were measured in real-time where an increase (*i.e.*, proliferation) or decrease (*i.e.*, cytotoxicity) in cell numbers correlates with an increase or decrease in cell index, respectively (Solly *et al.* 2004; Buontempo *et al.* 2011). Although the growth profiles for control cells were very similar (*i.e.*, superimposable), there was a dramatic difference within the *RAD54B*-deficient cells treated with either ATTM or 2ME2 (Figure 3B). In general, a large and reproducible decrease in the normalized cell indices occurred ~15–20 hr post-treatment (Figure 3B, right) and was typically completed within 5 hr. The rapid decreases in proliferation coupled with the lack of a "stationary" phase argues against a cell cycle arrest. In addition to the above data, statistically significant defects in proliferation (Figure 3C) were observed and strongly suggest that cellular cytotoxicity accounts for the decrease in cell numbers. Next, standard colony-formation assays were performed in which DMSO, ATTM, or 2ME2 were supplemented into the medium and colonies were permitted to grow for 28 days. As predicted, statistically significant decreases in the total number of *RAD54B*-deficient colonies treated with ATTM or 2ME2 occurred relative to controls (Figure 3D). Collectively, the above data indicate that ATTM and 2ME2 selectively target *RAD54B*-deficient cells over short (<4 days) and long (28 days) time frames and further support their roles as lead compounds for subsequent study.

ATTM and 2ME2 treatments induce ROS, persistent DNA double strand breaks, and apoptosis in RAD54B-deficient cells

ROS are chemically reactive oxygen molecules that cause oxidative stress, which frequently manifest as DNA double strand breaks (Higuchi 2003). In eukaryotes, this damage is normally repaired through two complementary repair pathways—nonhomologous end joining, which is "error prone," and homologous recombination repair, which is "error free." Since SOD1 is required for the removal of superoxide radicals, we postulated that SOD1 inhibition via ATTM, or increases in ROS following 2ME2 treatment, would produce DNA double strand breaks that normally would be repaired via the two functional DNA repair pathways. However, in *RAD54B*-deficient cells that are defective in homologous recombination repair, we predicted that the breaks will not be accurately repaired and will underlie the cellular cytotoxicity identified above.

Using live cell fluorescence microscopy, we first demonstrated that ATTM and 2ME2 induced ROS formation in both control and *RAD54B*-deficient cells relative to DMSO-treated controls (Figure 4). The prevalence and persistence of DNA double strand breaks was then evaluated at various

timepoints using two surrogate markers (γ-H2AX and 53BP1) for DNA double strand breaks (Rogakou *et al.* 1998). Semiquantitative imaging microscopy revealed visually apparent (Figure S4) and statistically significant increases in DNA-normalized γ-H2AX and 53BP1 signal intensities following a 6-hr treatment in both cell lines that did not occur within the DMSO-treated controls (Figure 5). Following washout and a 36-hr recovery period, the γ-H2AX and 53BP1 signal intensities remained elevated within the *RAD54B*-deficient cells but returned to basal levels within the control (Figure 5 and Table S6). Subsequent analysis of variance (ANOVA) confirmed statistically significant differences in the mean γ-H2AX and 53BP1 signal intensities following the ATTM and 2ME2 treatments in both cell lines (Table S7, Table S8, Table S9, and Table S10). Tukey's multicomparison post-tests revealed highly statistically significant increases in the mean γ-H2AX and 53BP1 total signal intensities between the untreated (t = 0 hr) and ATTM or 2ME2-treated cells following washout and recovery (t = 42 hr) within the *RAD54B*-deficient cells that were not significant within the controls (Table S11, Table S12, Table S13, and Table S14).

Although the above data show that *RAD54B*-deficient cells are hypersensitive to ATTM and 2ME2 treatments, they do not address the underlying mechanism. Images from our siRNA-based tests (Figure 2B) contained nuclei exhibiting classical apoptotic features such as chromatin condensation and nuclear blebbing. Consequently, we sought to determine whether apoptosis was a feature that contributed to the targeted killing of the *RAD54B*-deficient cells treated with ATTM or 2ME2. As predicted, semiquantitative imaging revealed a statistically significant increase in the abundance of cleaved Caspase 3 (apoptotic marker) only within the *RAD54B*-deficient cells treated with ATTM or 2ME2 relative to controls (Figure 6). These data show that ATTM and 2ME2 treatments induce apoptosis only within the *RAD54B*-deficient cells.

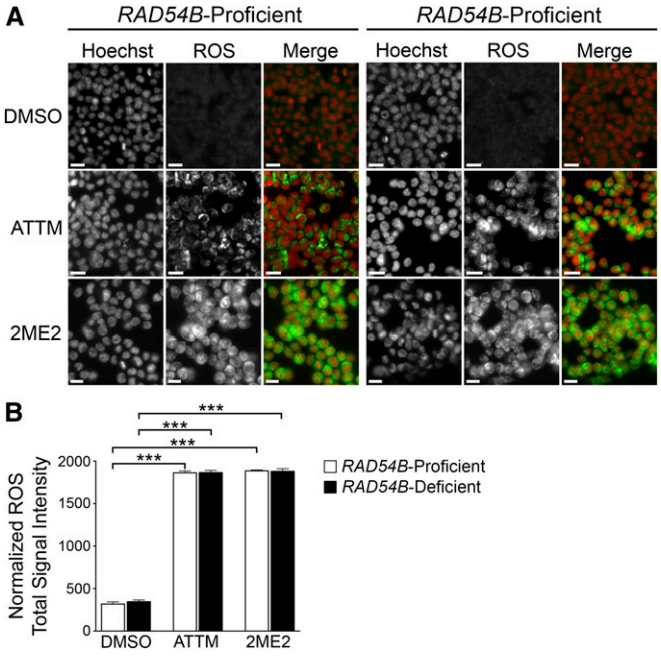

Figure 4 ATTM and 2ME2 treatments induce ROS production. (A) Representative images depicting the abundance of ROS as reflected by qualitative changes in the global abundance of fluorescein total signal intensity (green) in *RAD54B*-proficient and *RAD54B*-deficient cells treated with DMSO, ATTM, or 2ME2. All images were acquired using the identical exposure times and thus changes in fluorescence intensities reflect changes in the abundance of ROS in these cells. Images were acquired following a 6-hr incubation with the chemicals. Note that both *RAD54B*-proficient and *RAD54B*-deficient cells show an increase in ROS after treatment with ATTM or 2ME2. Nuclei (blue) are counterstained with Hoechst. Bar, 10 μm. (B) Graphical depiction of the changes in normalized ROS total signal intensity following DMSO, ATTM, and 2ME2 treatments (***P-value <0.0001).

Discussion

CRC has a significant health burden throughout the world and thus novel therapeutic strategies and targets are needed to minimize morbidity and mortality rates associated with the disease. Here we employ a cross-species approach to identify a highly connected, evolutionarily conserved SL interactor and confirm its potential as a novel candidate therapeutic target. Using bioinformatics and publicly available yeast SL datasets, we generated a genetic interaction dataset that was subsequently used to identify CIN gene/SL partner gene candidates to interrogate in a human CRC context. Preliminary direct tests revealed several SL interactions of *RAD54B* with genes involved in the removal of ROS, including *SOD1*. Using our established siRNA-based approach (McManus *et al.* 2009), we show that the yeast *RAD54 SOD1* SL interaction is conserved within two independent human cell lines. We further demonstrate that ATTM and 2ME2 can functionally substitute for the SOD1 siRNAs and decrease the number of *RAD54B*-deficient cells relative to controls in both short (<4 days) and longer-term assays (28 days). Finally, we provide evidence that ATTM and 2ME2 induce the formation of ROS and DNA double strand breaks that persist within the *RAD54B*-deficient cells that are associated with significant increases in cellular cytotoxicity and apoptosis. This study identifies and validates *SOD1* as an evolutionarily conserved SL interactor of *RAD54B* and thus confirms SOD1 as a novel candidate therapeutic target. The results of this study also support ATTM and 2ME2 as lead therapeutic compounds requiring subsequent preclinical study. Collectively, our data support the use of cross-species approaches to uncover evolutionarily conserved SL interactors that can be exploited as novel drug targets.

Although the SL targeting of *RAD54B*-deficient CRC cells through SOD1 inhibition is a novel therapeutic strategy, ATTM was originally employed by veterinarians to treat copper poisoning in livestock (Suttle 2012). In humans, ATTM has been employed to treat Wilson's disease, a neuropsychiatric disorder that results from the accumulation of Cu^{2+} within tissues (Brewer 2003), and most recently it has begun to be evaluated in various cancer contexts due to its ability to

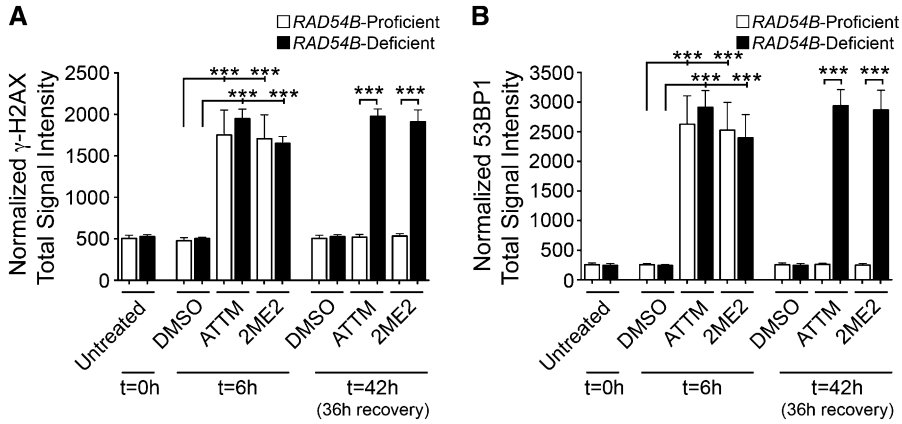

Figure 5 DNA double strand breaks persist in *RAD54B*-deficient cells following ATTM and 2ME2 treatment. (A) Graphs depicting the changes in normalized γ-H2AX total signal intensities in cells treated with DMSO, ATTM, or 2ME2. Semiquantitative imaging microscopy was performed on cells prior to treatment (t = 0 hr), following a 6-hr treatment (t = 6 hr), and following a 36-hr recovery, following washout (t = 42 hr) of drug (***P-value <0.0001). (B) Graphs depicting the semiquantitative changes in normalized 53BP1 total signal intensities following DMSO, ATTM, and 2ME2 treatments. Graphs are labeled as indicated in A.

adversely impact vascularization (angiogenesis), cell motility, and invasiveness (metastasis), and sensitize cancer cells to additional anticancer drugs (Pan *et al.* 2002; Henry *et al.* 2006; Gartner *et al.* 2009; Kumar *et al.* 2010; Kim *et al.* 2012). Indeed, several phase I and II clinical trails are currently underway to evaluate the efficacy of various Cu^{2+} chelators in a diverse array of tumor types including breast, esophageal, and prostate cancer (www.clinicaltrials.gov).

A SL therapeutic strategy represents a significant advancement over more traditional approaches that are not inherently designed to limit the therapeutic effect to cancer cells. For example, 5-FU and doxorubicin affect DNA replication, while paclitaxel affects mitosis and is associated with adverse side effects including neutropenia, cardiotoxicity, and infertility. The low concentrations of ATTM and 2ME2 employed in the *RAD54B SOD1* SL paradigm are purposefully selected to induce killing only within the *RAD54B*-deficient cells and are therefore not expected to produce side effects within normal surrounding cells. Indeed, the data presented above strongly suggest that control cells are minimally impacted following the transient administration of ATTM and 2ME2 as they are able to tolerate the transient increase in ROS and do not display any overt signs of unrepaired DNA double strand breaks or apoptosis. In fact, we predict that in addition to invoking SL killing of *RAD54B*-deficient cells, ATTM treatments may produce an additive or synergistic effect within tumors that stems from its potential role as an antiangiogenic and antimetastatic factor (Pan *et al.* 2002; Henry *et al.* 2006; Gartner *et al.* 2009; Kumar *et al.* 2010; Kim *et al.* 2012).

Recently, it was shown in HCT116 cells that *RAD54B* is SL with *LIG4* (Oh *et al.* 2013), which encodes DNA ligase IV, a key protein involved in nonhomologous end joining, and suggests that the homologous recombination repair and nonhomologous end joining pathways can functionally compensate for each other. However, the cytotoxic effects we observe within the *RAD54B*-deficient cells following SOD1 silencing or ATTM or 2ME2 treatments occur within the presence of a presumably functional nonhomologous end joining pathway. Although determining the exact mechanism(s) by which SOD1 silencing and ROS induction circumvents the nonhomologous end joining pathway is beyond the scope of the current study, it is possible that it induces a subset of DNA breaks that can only be repaired by the homologous recombination pathway such as those that occur in S-phase as a result of collapsed replication forks. However, it is also equally possible that the damage simply overwhelms the repair capacity of the nonhomologous end joining pathway, or alternatively that ROS induction induces signaling pathways that suppress nonhomologous end joining. In any case, these possibilities are speculative and remain to be evaluated.

When ROS overwhelm the antioxidant defenses of the host, free radicals can interact with various endogenous macromolecules and alter normal cellular function. If, for example, superoxide radicals are left unchecked, they will cause DNA double strand breaks, lipid peroxidation, and protein oxidation. Consequently, eukaryotes have evolved highly conserved mechanisms that are designed to minimize the impact of ROS. Of particular relevance to this study is the identification and clustering of three yeast genes *tsa1*, *ccs1*, and *sod1* (Figure 1A, bottom) and their corresponding human genes *PRDX2*, *CCS*, and *SOD1*, respectively, as common SL interactors for many yeast CIN genes whose human orthologs are somatically mutated in CRC. These three genes encode products that are required to remove superoxide radicals found within the cytoplasm through a two-step process. First, SOD1 dismutates superoxide radicals into another ROS, namely H_2O_2. SOD1 activity requires Cu^{2+} as an essential cofactor, which is normally provided via the SOD1 copper chaperone, CCS (Culotta *et al.* 1997). Next, peroxiredoxin (PRDX2) reduces H_2O_2 into water and oxygen. Although the current study focuses on SOD1 as a novel candidate therapeutic target, we provide preliminary evidence that suggests the two remaining components of this process, PRDX2 and CCS, may also possess therapeutic potential. For example, our initial siRNA-based screen of the mininetwork identified in Figure 1A suggests that *PRDX2* is a SL interactor with *RAD54B* and other genes somatically mutated in cancer (Figure 1C). Furthermore, our chemical studies demonstrate that ATTM, a chemical derivative of tetrathiomolybdate (ATN-224) (Juarez *et al.* 2006), selectively kills *RAD54B*-deficient cells (Figure 3). Although ATTM is a SOD1 inhibitor, it

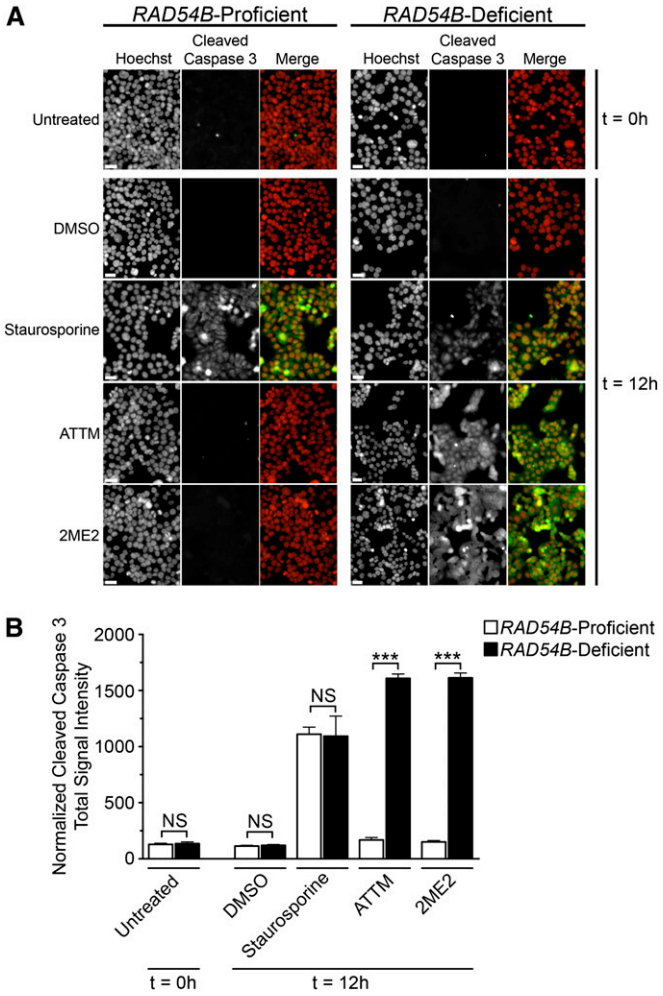

Figure 6 ATTM and 2ME2 selectively induce apoptosis in *RAD54B*-deficient cells. (A) Representative images depicting the abundance of apoptosis as reflected by qualitative increases in cleaved Caspase 3 in cells treated with DMSO, ATTM, or 2ME2. Staurosporine induces apoptosis and is included as a positive control. All images were acquired with identical exposure times and thus changes in fluorescence intensities identify changes in the global abundance of the cleaved Caspase 3 (apoptosis). Images were acquired immediately prior to treatment (t = 0 hr) and following a 12-hr treatment (t = 12 hr). The nuclei and cleaved Caspase 3 are pseudocolored red and green, respectively, within the merged images. Note the striking increase in cleaved Caspase 3 signal intensities within *RAD54B*-deficient cells treated with ATTM or 2ME2 relative to controls. Bar, 30 μm. (B) Graphs depicting the semiquantitative changes in the normalized cleaved Caspase 3 total signal intensities following DMSO, ATTM, and 2ME2 treatments (NS, not significant; ***P-value <0.0001). Quantitative imaging microscopy was performed on cells prior to treatment (t = 0 hr) and following a 12-hr treatment (t = 12 hr).

functions by chelating Cu^{2+}, an essential cofactor of SOD1. Consequently, it is plausible that the bioavailability of Cu^{2+} decreases following ATTM treatment, thus compromising the function of CCS as a copper chaperone for SOD1. Thus, targeting CCS chaperone activity may be of therapeutic benefit. In either case, validating and confirming PRDX2 and CCS as novel candidate targets will require subsequent study and goes beyond the scope of the current study.

The pharmacologic targeting of SOD1 has implications beyond the CRC-specific context described here. Although *RAD54B* is somatically mutated in ~3.3% of sporadic CRCs (Table S1) (Cancer Genome Atlas Network 2012), it is also somatically mutated and/or deleted in lymphoma, kidney, prostate, brain, and breast cancers (Hiramoto *et al.* 1999; Forbes *et al.* 2011; Cerami *et al.* 2012). In light of our findings that the *RAD54B SOD1* SL interaction is conserved within an immortalized fibroblast cell line (hTERT) (Figure 2D), SOD1 inhibition may be an effective therapeutic strategy to target and kill additional tumor types harboring *RAD54B* defects. It should also be noted that SOD1 inhibition might have broad-spectrum applicability beyond the *RAD54B*-specific paradigm presented here, as it is a member of the highly connected subset of SL partner genes described in this study. In yeast, *sod1* is SL with at least 41 different genes, and many like *rad54*, are involved in homologous recombination repair (Figure 1A). These genes, if conserved within a cancer context, may identify additional genetic defects that could be leveraged for therapeutic targeting. Indeed, our preliminary tests (Figure 1B) suggest this may be the case as a putative SL interaction was observed with *BLM*, a homologous recombination repair enzyme. *BLM* is somatically mutated in ~4.2% of CRCs as well as numerous other tumor types, including breast, lung, prostate, and ovarian (Table S1), and the relevance of therapeutically targeting SOD1 within these tumors warrants further study. In conclusion, we have presented data that rationalizes the use of cross-species approaches to assist in the identification of novel therapeutic targets designed to exploit somatic mutations causing CIN, for more selective and broader-spectrum targeting of cancer.

Acknowledgments

We thank John Wilkins (University of Manitoba) for microscope access. This work was funded by Canadian Institutes of Health Research (CIHR) operating grants (MOP-115179) to K.J.M. and (MOP-38096) to P.H., a Manitoba Health Research Council (MHRC)/CancerCare Manitoba fellowship to B.V.S., and a CIHR/MHRC new investigator award (to K.J.M.). M.B. is a trainee of the Michael Smith Foundation for Health Research.

Literature Cited

Barber, T. D., K. McManus, K. W. Yuen, M. Reis, G. Parmigiani *et al.*, 2008 Chromatid cohesion defects may underlie chromosome instability in human colorectal cancers. Proc. Natl. Acad. Sci. USA 105: 3443–3448.

Brewer, G. J., 2003 Tetrathiomolybdate anticopper therapy for Wilson's disease inhibits angiogenesis, fibrosis and inflammation. J. Cell. Mol. Med. 7: 11–20.

Buontempo, F., T. Ersahin, S. Missiroli, S. Senturk, D. Etro *et al.*, 2011 Inhibition of Akt signaling in hepatoma cells induces apoptotic cell death independent of Akt activation status. Invest. New Drugs 29: 1303–1313.

Cancer Genome Atlas Network, , 2012 Comprehensive molecular characterization of human colon and rectal cancer. Nature 487: 330–337.

Cerami, E., J. Gao, U. Dogrusoz, B. E. Gross, S. O. Sumer *et al.*, 2012 The cBio cancer genomics portal: an open platform for exploring multidimensional cancer genomics data. Cancer Discov. **2:** 401–404.

Chang, E. C., B. F. Crawford, Z. Hong, T. Bilinski, and D. J. Kosman, 1991 Genetic and biochemical characterization of Cu,Zn superoxide dismutase mutants in Saccharomyces cerevisiae. J. Biol. Chem. 266: 4417–4424.

Cogan, N., D. M. Baird, R. Phillips, L. A. Crompton, M. A. Caldwell *et al.*, 2010 DNA damaging bystander signalling from stem cells, cancer cells and fibroblasts after Cr(VI) exposure and its dependence on telomerase. Mutat. Res. 683: 1–8.

Culotta, V. C., L. W. Klomp, J. Strain, R. L. Casareno, B. Krems *et al.*, 1997 The copper chaperone for superoxide dismutase. J. Biol. Chem. 272: 23469–23472.

Dixon, S. J., Y. Fedyshyn, J. L. Koh, T. S. Prasad, C. Chahwan *et al.*, 2008 Significant conservation of synthetic lethal genetic interaction networks between distantly related eukaryotes. Proc. Natl. Acad. Sci. USA 105: 16653–16658.

Donate, F., J. C. Juarez, M. E. Burnett, M. M. Manuia, X. Guan *et al.*, 2008 Identification of biomarkers for the antiangiogenic and antitumour activity of the superoxide dismutase 1 (SOD1) inhibitor tetrathiomolybdate (ATN-224). Br. J. Cancer 98: 776–783.

Forbes, S. A., N. Bindal, S. Bamford, C. Cole, C. Y. Kok *et al.*, 2011 COSMIC: mining complete cancer genomes in the Catalogue of Somatic Mutations in Cancer. Nucleic Acids Res. 39: D945–D950.

Gao, C., K. Furge, J. Koeman, K. Dykema, Y. Su *et al.*, 2007 Chromosome instability, chromosome transcriptome, and clonal evolution of tumor cell populations. Proc. Natl. Acad. Sci. USA 104: 8995–9000.

Gartner, E. M., K. A. Griffith, Q. Pan, G. J. Brewer, G. F. Henja *et al.*, 2009 A pilot trial of the anti-angiogenic copper lowering agent tetrathiomolybdate in combination with irinotecan, 5-flurouracil, and leucovorin for metastatic colorectal cancer. Invest. New Drugs 27: 159–165.

Hartwell, L. H., P. Szankasi, C. J. Roberts, A. W. Murray, and S. H. Friend, 1997 Integrating genetic approaches into the discovery of anticancer drugs. Science 278: 1064–1068.

Heilig, C. E., H. Loffler, U. Mahlknecht, J. W. Janssen, A. D. Ho *et al.*, 2010 Chromosomal instability correlates with poor outcome in patients with myelodysplastic syndromes irrespectively of the cytogenetic risk group. J. Cell. Mol. Med. 14: 895–902.

Henry, N. L., R. Dunn, S. Merjaver, Q. Pan, K. J. Pienta *et al.*, 2006 Phase II trial of copper depletion with tetrathiomolybdate as an antiangiogenesis strategy in patients with hormone-refractory prostate cancer. Oncology 71: 168–175.

Higuchi, Y., 2003 Chromosomal DNA fragmentation in apoptosis and necrosis induced by oxidative stress. Biochem. Pharmacol. 66: 1527–1535.

Hiramoto, T., T. Nakanishi, T. Sumiyoshi, T. Fukuda, S. Matsuura *et al.*, 1999 Mutations of a novel human RAD54 homologue, RAD54B, in primary cancer. Oncogene 18: 3422–3426.

Huang, P., L. Feng, E. A. Oldham, M. J. Keating, and W. Plunkett, 2000 Superoxide dismutase as a target for the selective killing of cancer cells. Nature 407: 390–395.

Juarez, J. C., O. Betancourt, Jr., S. R. Pirie-Shepherd, X. Guan, M. L. Price *et al.*, 2006 Copper binding by tetrathiomolybdate attenuates angiogenesis and tumor cell proliferation through the inhibition of superoxide dismutase 1. Clin. Cancer Res. 12: 4974–4982.

Kachadourian, R., S. I. Liochev, D. E. Cabelli, M. N. Patel, I. Fridovich *et al.*, 2001 2-methoxyestradiol does not inhibit superoxide dismutase. Arch. Biochem. Biophys. 392: 349–353.

Kim, K. K., T. S. Lange, R. K. Singh, L. Brard, and R. G. Moore, 2012 Tetrathiomolybdate sensitizes ovarian cancer cells to anticancer drugs doxorubicin, fenretinide, 5-fluorouracil and mitomycin C. BMC Cancer 12: 147.

Kondo, T., A. G. Reaume, T. T. Huang, E. Carlson, K. Murakami *et al.*, 1997 Reduction of CuZn-superoxide dismutase activity exacerbates neuronal cell injury and edema formation after transient focal cerebral ischemia. J. Neurosci. 17: 4180–4189.

Kumar, P., A. Yadav, S. N. Patel, M. Islam, Q. Pan *et al.*, 2010 Tetrathiomolybdate inhibits head and neck cancer metastasis by decreasing tumor cell motility, invasiveness and by promoting tumor cell anoikis. Mol. Cancer 9: 206.

Lee, A. J., D. Endesfelder, A. J. Rowan, A. Walther, N. J. Birkbak *et al.*, 2011 Chromosomal instability confers intrinsic multidrug resistance. Cancer Res. 71: 1858–1870.

Lengauer, C., K. W. Kinzler, and B. Vogelstein, 1998 Genetic instabilities in human cancers. Nature 396: 643–649.

Lowndes, S. A., H. V. Sheldon, S. Cai, J. M. Taylor, and A. L. Harris, 2009 Copper chelator ATN-224 inhibits endothelial function by multiple mechanisms. Microvasc. Res. 77: 314–326.

McLellan, J., N. O'Neil, S. Tarailo, J. Stoepel, J. Bryan *et al.*, 2009 Synthetic lethal genetic interactions that decrease somatic cell proliferation in Caenorhabditis elegans identify the alternative RFC CTF18 as a candidate cancer drug target. Mol. Biol. Cell 20: 5306–5313.

McManus, K. J., and M. J. Hendzel, 2003 Quantitative analysis of CBP- and P300-induced histone acetylations in vivo using native chromatin. Mol. Cell. Biol. 23: 7611–7627.

McManus, K. J., and M. J. Hendzel, 2005 Using quantitative imaging microscopy to define the target substrate specificities of histone post-translational-modifying enzymes. Methods 36: 351–361.

McManus, K. J., I. J. Barrett, Y. Nouhi, and P. Hieter, 2009 Specific synthetic lethal killing of RAD54B-deficient human colorectal cancer cells by FEN1 silencing. Proc. Natl. Acad. Sci. USA 106: 3276–3281.

Miyagawa, K., T. Tsuruga, A. Kinomura, K. Usui, M. Katsura *et al.*, 2002 A role for RAD54B in homologous recombination in human cells. EMBO J. 21: 175–180.

Oh, S., Y. Wang, J. Zimbric, and E. A. Hendrickson, 2013 Human LIGIV is synthetically lethal with the loss of Rad54B-dependent recombination and is required for certain chromosome fusion events induced by telomere dysfunction. Nucleic Acids Res. 41: 1734–1749.

Pan, Q., C. G. Kleer, K. L. van Golen, J. Irani, K. M. Bottema *et al.*, 2002 Copper deficiency induced by tetrathiomolybdate suppresses tumor growth and angiogenesis. Cancer Res. 62: 4854–4859.

Pan, X., P. Ye, D. S. Yuan, X. Wang, J. S. Bader *et al.*, 2006 A DNA integrity network in the yeast Saccharomyces cerevisiae. Cell 124: 1069–1081.

Rajagopalan, H., P. V. Jallepalli, C. Rago, V. E. Velculescu, K. W. Kinzler *et al.*, 2004 Inactivation of hCDC4 can cause chromosomal instability. Nature 428: 77–81.

Rogakou, E. P., D. R. Pilch, A. H. Orr, V. S. Ivanova, and W. M. Bonner, 1998 DNA double-stranded breaks induce histone H2AX phosphorylation on serine 139. J. Biol. Chem. 273: 5858–5868.

Shih, I. M., W. Zhou, S. N. Goodman, C. Lengauer, K. W. Kinzler *et al.*, 2001 Evidence that genetic instability occurs at an early stage of colorectal tumorigenesis. Cancer Res. 61: 818–822.

Sjoblom, T., S. Jones, L. D. Wood, D. W. Parsons, J. Lin *et al.*, 2006 The consensus coding sequences of human breast and colorectal cancers. Science 314: 268–274.

Solly, K., X. Wang, X. Xu, B. Strulovici, and W. Zheng, 2004 Application of real-time cell electronic sensing (RT-CES)

technology to cell-based assays. Assay Drug Dev. Technol. 2: 363–372.
Spankuch-Schmitt, B., J. Bereiter-Hahn, M. Kaufmann, and K. Strebhardt, 2002 Effect of RNA silencing of polo-like kinase-1 (PLK1) on apoptosis and spindle formation in human cancer cells. J. Natl. Cancer Inst. 94: 1863–1877.
Stirling, P. C., M. S. Bloom, T. Solanki-Patil, S. Smith, P. Sipahimalani *et al.*, 2011 The complete spectrum of yeast chromosome instability genes identifies candidate CIN cancer genes and functional roles for ASTRA complex components. PLoS Genet. 7: e1002057.
Suttle, N. F., 2012 Copper imbalances in ruminants and humans: unexpected common ground. Adv Nutr 3: 666–674.
Tarailo, M., S. Tarailo, and A. M. Rose, 2007 Synthetic lethal interactions identify phenotypic "interologs" of the spindle assembly checkpoint components. Genetics 177: 2525–2530.
Tong, A. H., M. Evangelista, A. B. Parsons, H. Xu, G. D. Bader *et al.*, 2001 Systematic genetic analysis with ordered arrays of yeast deletion mutants. Science 294: 2364–2368.
van Pel, D. M., I. J. Barrett, Y. Shimizu, B. V. Sajesh, B. J. Guppy *et al.*, 2013 An evolutionarily conserved synthetic lethal interaction network identifies FEN1 as a broad-spectrum target for anticancer therapeutic development. PLoS Genet. 9: e1003254.
Wang, Z., J. M. Cummins, D. Shen, D. P. Cahill, P. V. Jallepalli *et al.*, 2004 Three classes of genes mutated in colorectal cancers with chromosomal instability. Cancer Res. 64: 2998–3001.
Yuen, K. W., C. D. Warren, O. Chen, T. Kwok, P. Hieter *et al.*, 2007 Systematic genome instability screens in yeast and their potential relevance to cancer. Proc. Natl. Acad. Sci. USA 104: 3925–3930.

Communicating editor: J. Nickoloff

GENETICS

Supporting Information
http://www.genetics.org/lookup/suppl/doi:10.1534/genetics.113.156836/-/DC1

Synthetic Lethal Targeting of Superoxide Dismutase 1 Selectively Kills *RAD54B*-Deficient Colorectal Cancer Cells

Babu V. Sajesh, Melanie Bailey, Zelda Lichtensztejn, Philip Hieter, and Kirk J. McManus

DOI: 10.1534/genetics.113.156836

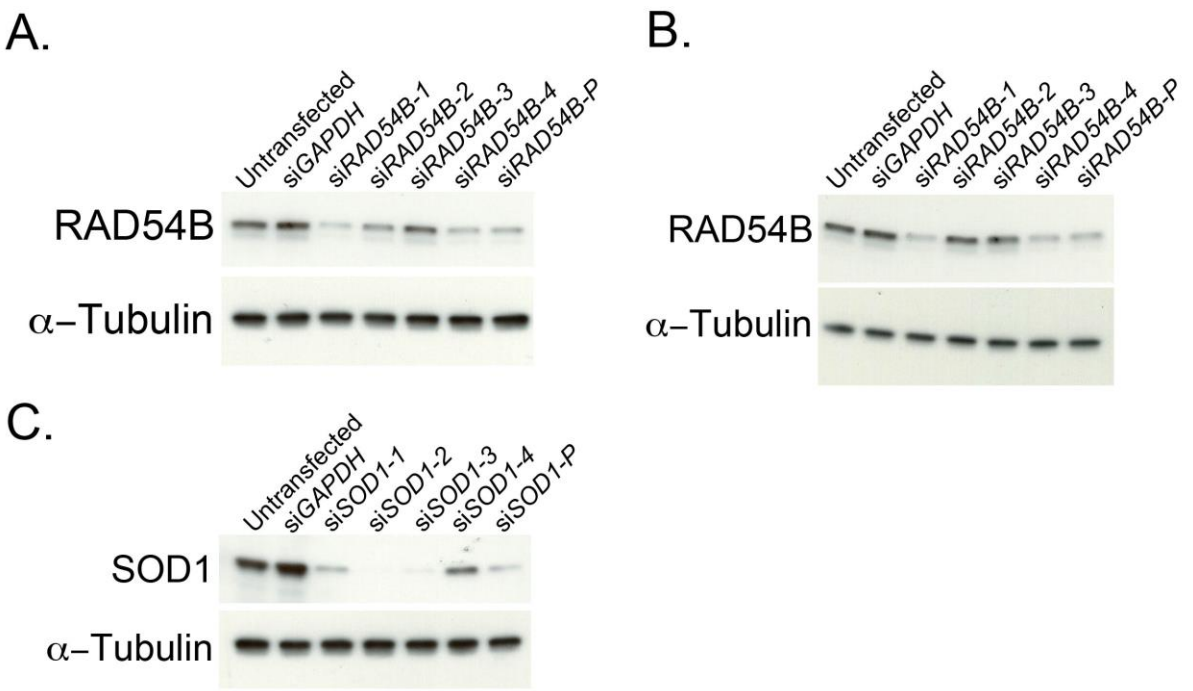

Figure S1 Efficiency of siRNA-based silencing in human cells. (A) Representative Western blot depicting the level of silencing achieved following RAD54B silencing in HCT116 (*RAD54B*-proficient) cells. Conditions and siRNAs are indicated above the individual lanes: α-tubulin is used as a loading control. (B) Representative Western blot depicting the level of silencing achieved following RAD54B silencing in hTERT cells. (C) Representative Western blot depicting the level of silencing achieved following SOD1 silencing in hTERT cells.

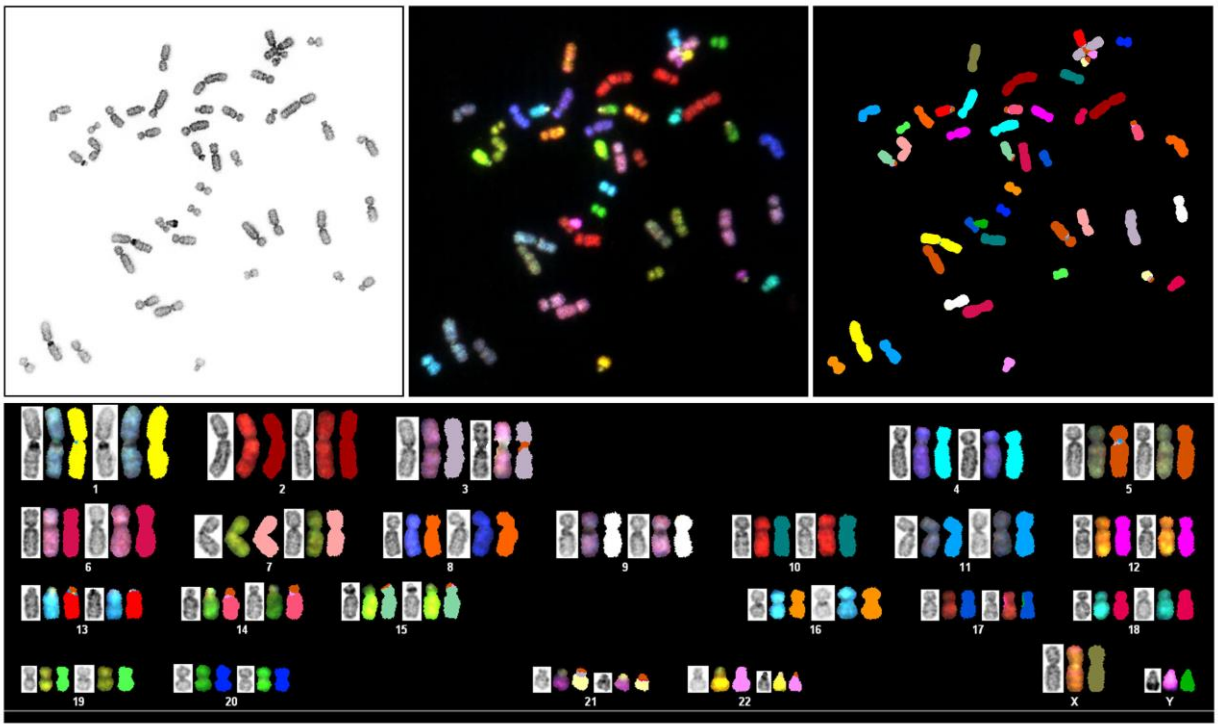

Figure S2 Spectral karyotyping (SKY) reveals a diploid karyotype for hTERT cells. Representative SKY image of a typical mitotic chromosome spread prepared from hTERT cells. Presented are the inverted DAPI image (top left), the raw spectral image (top middle), and the SKY classified image (top right) for the original spread. The classified karyotype is presented (bottom) with the individual chromosome numbers indicated. Each karyotyped chromosome is presented in the 3 formats; inverted DAPI (left), raw spectrum (middle) and SKY classified (right).

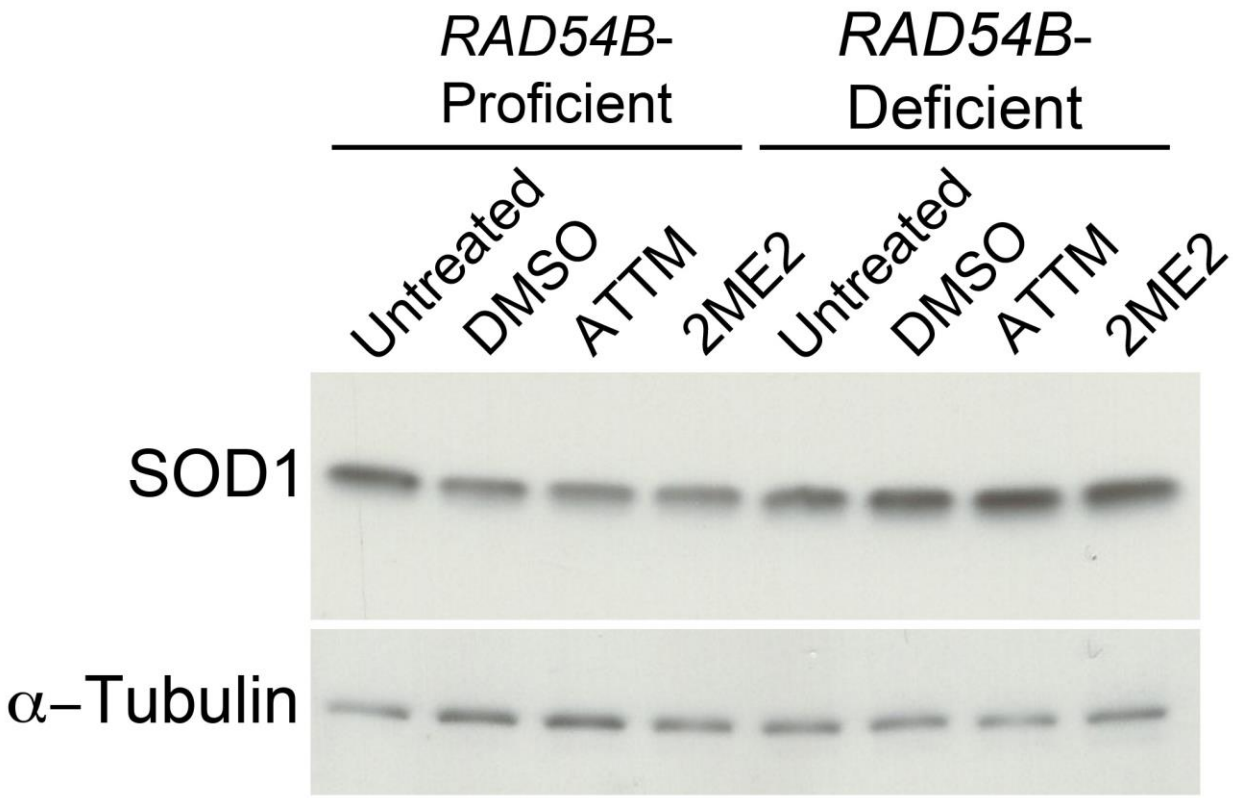

Figure S3 SOD1 expression levels following treatment with ATTM and 2ME2. Representative Western blot depicting the SOD1 expression levels in both *RAD54B*-proficient (left) and *RAD54B*-deficient (right) cells treated with DMSO, ATTM and 2ME2 for 12h relative to untreated; α-tubulin is included as a loading control.

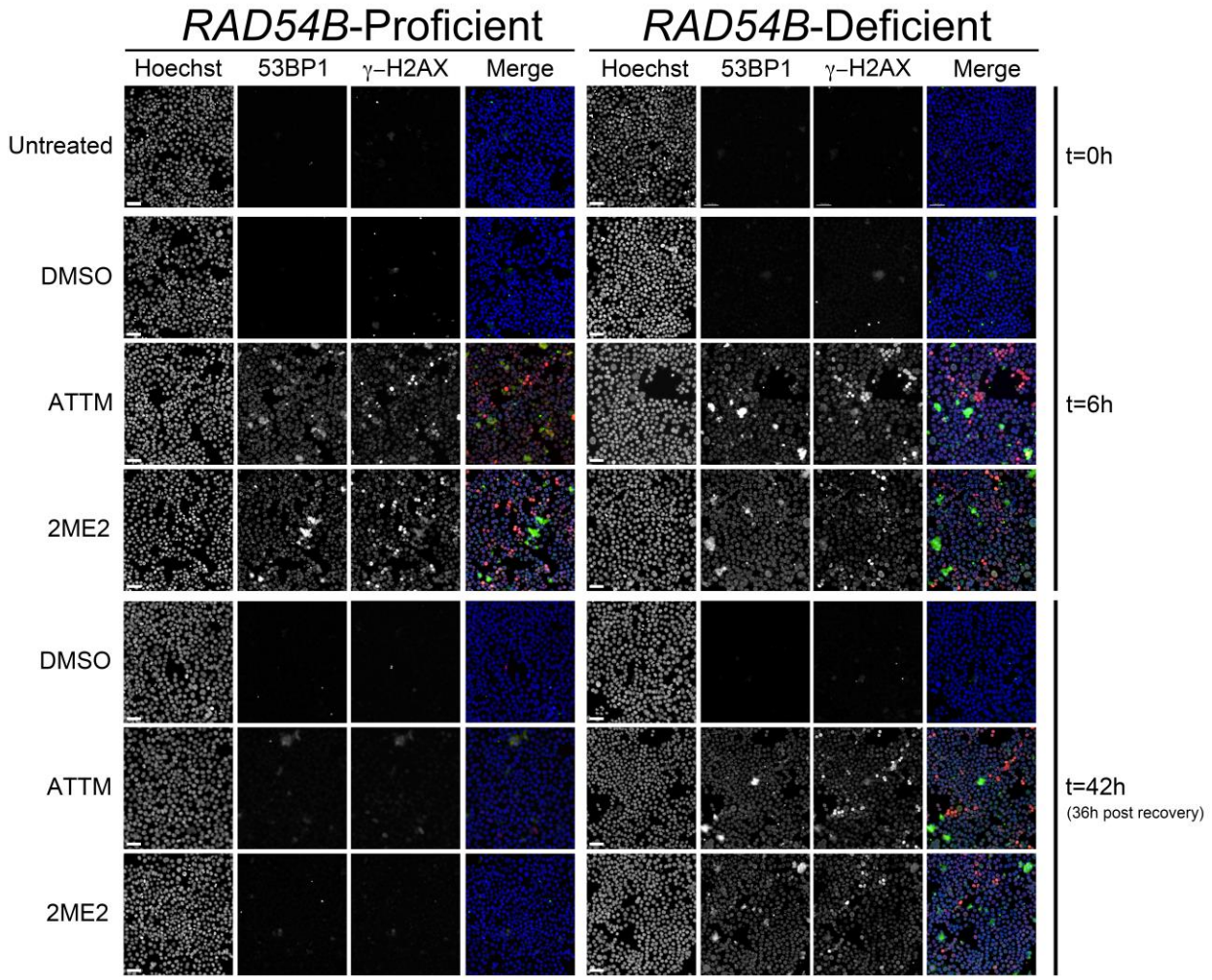

Figure S4 DNA double strand breaks persist in *RAD54B*-deficient cells following SOD1 inhibition. Representative images depicting the abundance of DNA double strand breaks as reflected by qualitative changes in the global abundance of 53BP1 (green) and γ-H2AX (red) in *RAD54B*-proficient and *RAD54B*-deficient cells treated with DMSO, ATTM or 2ME2. All images were acquired using the identical exposure times and thus changes in fluorescence intensities reflect changes in the global abundance of the specific epitopes evaluated. Images were acquired immediately prior to chemical addition (t = 0h), following a 6h incubation with the chemicals (t = 6h), and following a 36h recovery phase in the absence of any chemical (t = 42h). Note the persistence of both the 53BP1 and γ-H2AX signals within the *RAD54B*-deficient cells treated with either ATTM or 2ME2 that were permitted to recover (t = 42h), relative to the corresponding *RAD54B*-proficient controls. Nuclei (blue) are counterstained with Hoechst. Scale bar represents 50μm.

Table S1 Human Orthologs of Yeast Genetic Interactors are Frequently Altered in Human Cancers

Yeast Protein	Human Protein[A]	Human Accession	E-Value	Frequency in CRC[B]	Other Cancers[C]
MEC1	ATR	NP_001175.2	0.0	7.1%	BR, GB, L, S, SO
RAD53	CHEK2	NP_009125.1	2.00E-101	0.5%	BR, GB, L, SO
RAD59	RAD52	NP_602296.2	1.00E-45	1.9%	BR, L, P, S
DIA2	none	N/A	N/A	N/A	N/A
RFA1	RPA1	NP_002936.1	0.0	0.9%	BR, L, S, SO
RNR4	RRM2	NP_001159403.1	1.00E-144	0.5%	BR, L
RAD18	RAD18	NP_064550.3	1.00E-31	1.4%	BR, L, SO
RAD5	HLTF	NP_003062.2	2.00E-107	1.9%	BR, L
DUN1	CHEK2	NP_001005735.1	1.00E-109	0.5%	BR, GB, L, SO
CTF4	WDR69	NP_849143.1	1.00E-50	2.4%	BR, L, P, SO
	WDHD1[†]	NP_009017.1	N/A	2.4%	BR, L SO
CTF8	CHTF8	NP_001034779.1	3.00E-19	0.0%	BR, SO
CTF18	CHTF18[†]	NP_071375.1	4.00E-36	0.0%	BR, L, SO
DCC1	DSCC1	NP_076999.2	8.00E-97	0.5%	SO
POL32	POLD3[†]	NP_006582.1	N/A	0.9%	L, S, SO
RAD27	FEN1	NP_004102.1	6.00E-167	2.4%	BR, SO
ELG1	RFC1	NP_001191676.1	6.00E-28	4.2%	BR, L, SO
	ATAD5[†]	NP_079133.3	2.00E-05	4.2%	BR, L, SO
MRC1	MYO18A	NP_976063.1	1.00E-14	1.9%	BR, L, SO
	CLSPN[†]	NP_071394.2	N/A	2.4%	BR, L, SO
TOF1	TIMELESS	NP_003911.2	9.00E-77	2.4%	BR, L, SO
CSM3	TIPIN	NP_060328.2	8.00E-26	0.5%	BR, SO
RAD51	RAD51	NP_002866.2	3.00E-147	0.5%	BR, L, SO
RAD54	RAD54L	NP_003570.2	5.00E-133	1.4%	BR, L, SO
	RAD54B[†]	NP_036547.1	1.00E-121	3.3%	BR, L, SO
RAD55	RAD51	NP_002866.2	1.00E-45	0.5%	BR, L, SO
RAD57	RAD51	NP_002866.2	4.00E-83	0.5%	BR, L, SO
RAD52	RAD52	NP_602296.2	1.00E-58	2.4%	BR, L, P, S
RAD50	RAD50	NP_005723.2	5.00E-67	6.6%	BR, L, P, SO
XRS2	NBN	NP_002476.2	N/A	0.9%	BR, GB, L, SO
MRE11	MRE11A	NP_005581.2	2.00E-136	1.9%	BR, L
RTT107	PAXIP1	NP_0311375.3	8.00E-21	1.9%	BR, L, P, SO
SRS2	IGHMBP2	NP_002171.2	7.00E-17	1.9%	L
SGS1	WRN	NP_000544.2	3.00E-134	4.7%	BR, L, P, S, SO
	BLM[†]	NP_000048.1	4.00E-128	4.2%	BR, L, P, SO

[A]DELTA-BLAST (protein) searches were conducted to identify the real or putative human orthologs of yeast genetic interacting proteins identified in Fig. 1A (bottom). The top-ranked human candidates (based on E-value) for each are shown. In instances where the known ortholog was not identified based on protein sequence alignment, the corresponding functional ortholog has been included and is identified ([†]).

[B]cBio Cancer Genomics Portal (http://www.cbioportal.org/public-portal/) was queried for the frequency of colorectal cancer (CRC) tumors harboring only non-synonymous single nucleotide polymorphisms or homozygous deletions – gene amplifications were purposefully excluded. Data is compiled from a total of 212 unique tumor samples.

[C]Additional tumor types from cBio Cancer Genomics Portal for which there were studies with mutation data (harboring nsSNPs or homozygous deletions) were also queried and include; breast invasive carcinoma (BR), glioblastoma (GB), lung squamous cell carcinoma (L), prostate cancer (P), sarcoma (S), and serous ovarian cancer (SO).

Table S2 Statistical analysis of synthetic lethal interaction between SOD1 and RAD54B[A].

		Mean Cell Number ± SD[C]		
siRNA Treatment	N[B]	*RAD54B*-proficient	*RAD54B*-deficient	*p*-value
si*GAPDH*	6	4795 ± 44.1	4756 ± 48.1	1.72E-01
si*SOD1-P*	6	4674 ± 40.5	2372 ± 38.4	2.22E-16
si*SOD1-2*	6	4661 ± 49.7	1312 ± 60.7	1.56E-16
si*SOD1-3*	6	4736 ± 41.8	1323 ± 90.2	1.39E-15
si*PLK1*	6	17 ± 8.2	20.33 ± 5.3	4.21E-01

[A]Only a single representative example of an experiment conducted in sextuplet is shown. Each experiment was repeated 2 additional times with similar results.
[B]N; number of wells analyzed
[C]SD; standard deviation

Table S3 Dual siRNA-based SL Testing in HCT116 Cells.

siRNA Treatment	N[A]	Mean ± SD[B]	Normalized Relative %[C]	Expected %[D]	Difference (%)[E]
si*GAPDH*	6	4790 ± 97.4	100.0	N/A	N/A
si*RAD54B*	6	4444 ± 48.8	92.8	N/A	N/A
si*SOD1-P*	6	4396 ± 50.1	91.8	N/A	N/A
si*SOD1-2*	6	4421 ± 69.1	92.3	N/A	N/A
si*SOD1-3*	6	4410 ± 30.8	92.1	N/A	N/A
si*RAD54B* + si*SOD1-P*	6	3441 ± 95.0	71.8	85.1	15.6
si*RAD54B* + si*SOD1-2*	6	3309 ± 88.0	69.1	85.6	19.3
si*RAD54B* + si*SOD1-3*	6	3353 ± 126.4	70.0	85.4	18.0
si*PLK1*	6	246 ± 107.5	5.1	N/A	N/A

[A]N; number of wells analyzed
[B]SD; standard deviation
[C]All values are normalized to the si*GAPDH* control
[D]Calculated by multiplying the Normalized Relative % of the two individual siRNAs
[E]Calculated as 1 - (Normalized Relative %/Expected %) × 100 (N/A; not applicable)

Table S4 Spectral Karyotype of hTERT Cells at Various Passage Numbers.

Cell Line	Passage No.	N	Modal Chromosome Number [%[A]]	Karyotype [%[A]]
hTERT	3	69	46 [100%]	46,XY [69.7%] or 46,XY,t(X;3) [30.4%]
hTERT	20	67	46 [100%]	46,XY [13.4%] or 46,XY,t(X;3) [86.6%]
hTERT	34	67	46 [100%]	46,XY [14.9%] or 46,XY,t(X;3) [85.1%]

[A]the frequency of mitotic spreads with the corresponding karyotype

Table S5 Dual siRNA-based SL Testing in hTERT Cells.

siRNA Treatment	N[A]	Mean ± SD[B]	Normalized Relative %[C]	Expected %[D]	Difference (%)[E]
si*GAPDH*	6	965.3 ± 51.9	100.0	N/A	N/A
si*RAD54B*	6	912.8 ± 29.7	94.6	N/A	N/A
si*SOD1-P*	6	908.8 ± 14.8	94.1	N/A	N/A
si*SOD1-2*	6	865.5 ± 61.6	89.7	N/A	N/A
si*SOD1-3*	6	904.8 ± 59.0	93.7	N/A	N/A
si*RAD54B* + si*SOD1-P*	6	591.0 ± 32.8	61.2	89.0	31.2
si*RAD54B* + si*SOD1-2*	6	557.8 ± 42.1	57.8	84.8	31.8
si*RAD54B* + si*SOD1-3*	6	577.0 ± 83.2	59.8	88.6	32.6
si*PLK1*	6	56.7 ± 13.1	5.9	N/A	N/A

[A]N; number of wells analyzed
[B]SD; standard deviation
[C]All values are normalized to the si*GAPDH* control
[D]Calculated by multiplying the Normalized Relative % of the two individual siRNAs
[E]Calculated as 1 - (Normalized Relative %/Expected %) × 100 (N/A; not applicable)

Table S6 Fold Increase in γ-H2AX and 53BP1 Signal Intensities Following ATTM and 2ME2 Treatments.

		Fold Increase in Normalized Total Signal Intensity[A]			
		RAD54B-proficient		*RAD54B*-deficient	
Timepoint	Drug	γ-H2AX	53BP1	γ-H2AX	53BP1
t = 6h	ATTM	3.47	10.29	3.70	11.92
	2ME2	3.38	9.90	3.14	9.81
t = 42h	ATTM	1.03	1.02	3.75	12.03
	2ME2	1.06	0.97	3.63	11.74

[A]Fold increase is calculated by comparing the normalized total signal intensities for either γ-H2AX or 53BP1 to the corresponding condition and cell line at t = 0h.

Table S7 Analysis of Variance for Mean γ-H2AX Signal Intensities in *RAD54B*-proficient Cells Treated with DMSO, ATTM and 2ME2.

Group[A]	SS[B]	df[C]	MS[D]	F-ratio[E]	*p*-value	Reject H_0[F]
BG	1.29×10^7	6	2.15×10^6	82.30	<0.0001	Yes
WG	9.24×10^5	35	$2.61\text{x}10^4$			

[A]Defines whether or not the analysis is between groups/treatments (BG) or within the group/treatment (WG).
[B]Sum of Squares
[C]Degrees of freedom
[D]Mean square
[E]Calculated by MS_{BG}/MS_{WG}
[F]The null hypothesis (H_0) is rejected if the *p*-value is <0.05

Table S8 Analysis of Variance for Mean γ-H2AX Signal Intensities in *RAD54B*-deficient Cells Treated with DMSO, ATTM and 2ME2.

Group[A]	SS[B]	df[C]	MS[D]	F-ratio[E]	*p*-value	Reject H_0[F]
BG	1.92×10^7	6	3.20×10^6	331.0	<0.0001	Yes
WG	3.38×10^5	35	9.66×10^3			

[A]Defines whether or not the analysis is between groups/treatments (BG) or within the group/treatment (WG).
[B]Sum of Squares
[C]Degrees of freedom
[D]Mean square
[E]Calculated by MS_{BG}/MS_{WG}
[F]The null hypothesis (H_0) is rejected if the *p*-value is <0.05

Table S9 Analysis of Variance for Mean 53BP1 Signal Intensities in *RAD54B*-proficient Cells Treated with DMSO, ATTM and 2ME2.

Group[A]	SS[B]	df[C]	MS[D]	F-ratio[E]	*p*-value	Reject H_0[F]
BG	4.61×10^7	6	7.74×10^6	120.2	<0.0001	Yes
WG	2.25×10^6	35	6.43×10^4			

[A]Defines whether or not the analysis is between groups/treatments (BG) or within the group/treatment (WG).
[B]Sum of Squares
[C]Degrees of freedom
[D]Mean square
[E]Calculated by MS_{BG}/MS_{WG}
[F]The null hypothesis (H_0) is rejected if the *p*-value is <0.05

Table S10 Analysis of Variance for Mean 53BP1 Signal Intensities in *RAD54B*-deficient Cells Treated with DMSO, ATTM and 2ME2.

Group[A]	SS[B]	df[C]	MS[D]	F-ratio[E]	*p*-value	Reject H_0[F]
BG	6.74×10^7	6	1.12×10^7	185.5	<0.0001	Yes
WG	2.12×10^6	35	6.06×10^4			

[A]Defines whether or not the analysis is between groups/treatments (BG) or within the group/treatment (WG).
[B]Sum of Squares
[C]Degrees of freedom
[D]Mean square
[E]Calculated by MS_{BG}/MS_{WG}
[F]The null hypothesis (H_0) is rejected if the *p*-value is <0.05

Table S11 Tukey Multicomparison Post-test for Differences in γ-H2AX Signal Intensities in *RAD54B*-proficient Cells Treated with DMSO, ATTM and 2ME2.

	DMSO (6h)	ATTM (6h)	2ME2 (6h)	DMSO (42h)	ATTM (42h)	2ME2 (42h)
Untreated (0h)	NS[A]	****	****	NS	NS	NS
DMSO (6h)	-	****	****	NS	NS	NS
ATTM (6h)	-	-	NS	****	****	****
2ME2 (6h)	-	-	-	****	****	****
DMSO (42h)	-	-	-	-	NS	NS
ATTM (42h)	-	-	-	-	-	NS

[A]Not statistically significant (NS; *p*-value >0.05), low statistical significance (*; *p*-value <0.05), moderate statistical significance (**; *p*-value <0.01), high statistical significance (***; *p*-value <0.001), and very high statistical significance (****; *p*-value <0.0001).

Table S12 Tukey Multicomparison Post-test for Differences in γ-H2AX Signal Intensities in *RAD54B*-deficient Cells Treated with DMSO, ATTM and 2ME2.

	DMSO (6h)	ATTM (6h)	2ME2 (6h)	DMSO (42h)	ATTM (42h)	2ME2 (42h)
Untreated (0h)	NS	****	****	NS	****	****
DMSO (6h)	-	****	****	NS	****	****
ATTM (6h)	-	-	***	****	NS	NS
2ME2 (6h)	-	-	-	****	****	**
DMSO (42h)	-	-	-	-	****	****
ATTM (42h)	-	-	-	-	-	NS

[A]Not statistically significant (NS; *p*-value >0.05), low statistical significance (*; *p*-value <0.05), moderate statistical significance (**; *p*-value <0.01), high statistical significance (***; *p*-value <0.001), and very high statistical significance (****; *p*-value <0.0001).

Table S13 Tukey Multicomparison Post-test for Differences in 53BP1 Signal Intensities in *RAD54B*-proficient Cells Treated with DMSO, ATTM and 2ME2.

	DMSO (6h)	ATTM (6h)	2ME2 (6h)	DMSO (42h)	ATTM (42h)	2ME2 (42h)
Untreated (0h)	NS	****	****	NS	NS	NS
DMSO (6h)	-	****	****	NS	NS	NS
ATTM (6h)	-	-	NS	****	****	****
2ME2 (6h)	-	-	-	****	****	****
DMSO (42h)	-	-	-	-	NS	NS
ATTM (42h)	-	-	-	-	-	NS

[A]Not statistically significant (NS; *p*-value >0.05), low statistical significance (*; *p*-value <0.05), moderate statistical significance (**; *p*-value <0.01), high statistical significance (***; *p*-value <0.001), and very high statistical significance (****; *p*-value <0.0001).

Table S14 Tukey Multicomparison Post-test for Differences in 53BP1 Signal Intensities in *RAD54B*-deficient Cells Treated with DMSO, ATTM and 2ME2.

	DMSO (6h)	ATTM (6h)	2ME2 (6h)	DMSO (42h)	ATTM (42h)	2ME2 (42h)
Untreated (0h)	NS	****	****	NS	****	****
DMSO (6h)	-	****	****	NS	****	****
ATTM (6h)	-	-	*	****	NS	NS
2ME2 (6h)	-	-	-	****	**	*
DMSO (42h)	-	-	-	-	****	****
ATTM (42h)	-	-	-	-	-	NS

[A]Not statistically significant (NS; *p*-value >0.05), low statistical significance (*; *p*-value <0.05), moderate statistical significance (**; *p*-value <0.01), high statistical significance (***; *p*-value <0.001), and very high statistical significance (****; *p*-value <0.0001).